COMPENSATION OF MEASURED FREQUENCY RESPONSE FUNCTIONS USING ACCELEROMETER MODELS AND INVERSE RCSA

Harsha Satyanarayana and Tony L. Schmitz
Mechanical Engineering and Engineering Science
University of North Carolina at Charlotte, Charlotte, NC

INTRODUCTION

Machining operations may be stable or unstable depending on the cutting parameters and machine-spindle-holder-tool assembly frequency response function (FRF). Stable cutting conditions can be predicted using analytical stability models [1-3]. These models require knowledge of the assembly FRF and the cutting force model. The FRF can be obtained by measurement or modelling. For the latter, Schmitz and Donaldson [4] first presented the Receptance Coupling Substructure Analysis (RCSA) method to predict the machine-spindle-holder-tool FRFs by coupling individual component FRFs (or receptances). This method reduces measurement time because assembly FRFs can be predicted rather than measured. Subsequent efforts by the authors have improved the technique [5-14].

In this paper, another novel application of RCSA is presented to improve FRF measurement accuracy. In modal testing the tool tip FRF is measured using an instrumented hammer to excite the structure and an accelerometer to record the corresponding response. However, the measured FRF is slightly different than the actual tool tip FRF due to the accelerometer mass and cable effects. Mass loading compensation has been previously studied in [15-17]. To build on these prior efforts and compensate for both mass loading and cable damping, the inverse RCSA approach is applied here. In this approach, a model of the accelerometer-cable is decoupled from the measured FRF to isolate the structure's FRF. Experimental results are presented for three setups: 1) 12.7 mm diameter cantilever rod; 2) 6.35 mm diameter cantilever rod; and 3) clamped-clamped-clamped-free boundary condition thin ribs.

RCSA BACKGROUND

RCSA is a powerful tool for predicting assembly receptances, or FRFs, using individual component receptances. The component receptances obtained from measurements or modelling (analytical or numerical) are coupled using appropriate connection parameters to predict the assembly receptance [1]. The coupling might be rigid, flexible, or flexible-damped based on the assembly configuration [18]; see Fig. 1.

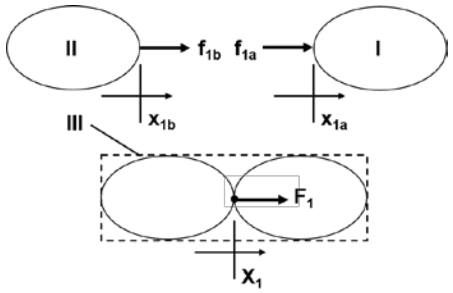

Figure 1. Two component RCSA model: I and II are individual components while III is assembly of I and II.

The components' direct receptances can be described as $h_{1a1a} = \frac{x_{1a}}{f_{1a}}$ and $h_{1b1b} = \frac{x_{1b}}{f_{1b}}$ for components I and II, respectively. The compatibility condition for rigid coupling is defined to be $x_{1b} - x_{1a} = 0$. The equilibrium condition, $f_{1a} + f_{1b} = F_1$, must also be described in order to equate the sum of internal (component) forces to the external (assembly) force. Finally, the assembly direct receptance at coordinate X_1 can be expressed as shown in Eq. 1.

$$H_{11} = \frac{X_1}{F_1} = h_{1a1a} - h_{1a1a}(h_{1a1a} + h_{1b1b})^{-1} h_{1a1a} \quad (1)$$

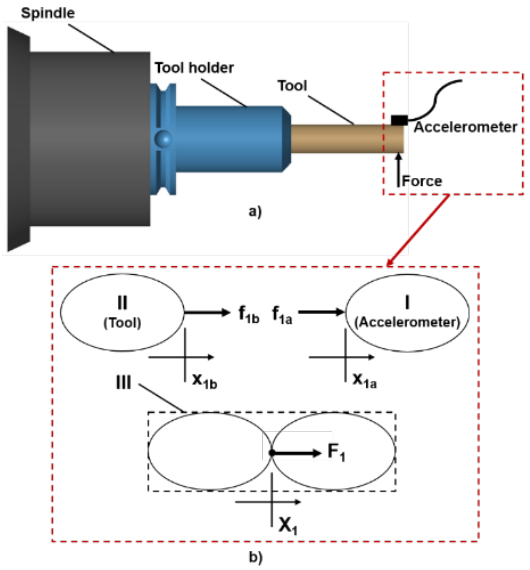

Figure 2. FRF measurement and the RCSA model.

INVERSE RCSA FOR MEASURED RECEPTANCE COMPENSATION

Tool tip receptances are often measured using an instrumented hammer to excite the structure and a low-mass accelerometer to measure the response to the applied force (Fig. 2a). However, the experimental receptance is different from the actual tool tip receptance due to the accelerometer mass and cable effects. The mass and cable effect can be compensated using inverse RCSA. Figure 2b shows the RCSA model for the accelerometer-tool assembly. In the model, it is assumed that the accelerometer is rigidly coupled to the tool tip.

The measured assembly receptance is $H_{11} = \frac{X_1}{F_1}$.The accelerometer and tool's direct receptances are described as $h_{1a1a} = \frac{x_{1a}}{f_{1a}}$ and $h_{1b1b} = \frac{x_{1b}}{f_{1b}}$, respectively. Using inverse RCSA, the actual tool tip receptance, h_{1b1b}, is:

$$h_{1b1b} = -h_{1a1a} + h_{1a1a}(h_{1a1a} - H_{11})^{-1}h_{1a1a} \qquad (2)$$

The accelerometer receptance is defined to be $h_{1a1a} = \frac{1}{-m\omega^2 + ic\omega}$, where *m* is the accelerometer mass and *c* is the viscous damping coefficient that quantifies the cable's energy dissipation. Note that *c* can be set to zero if damping compensation is not desired.

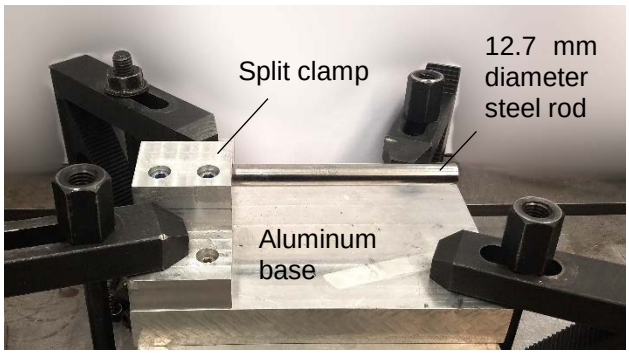

Figure 3. 12.7 mm diameter rod setup.

RESULTS

Experiments were performed on two setups: 12.7 mm diameter and 6.35 mm diameter steel rods with clamped-free boundary conditions. Figure 3 displays a photograph of the 12.7 mm diameter rod measurement platform. A split clamp was used to hold the rod at the desired cantilever length. The 6.35 mm diameter rod was clamped in an ER16 collet holder with a CAT-40 interface, which was then secured using a manual draw bolt in a spindle nose attached to a large steel block; see Fig. 4.

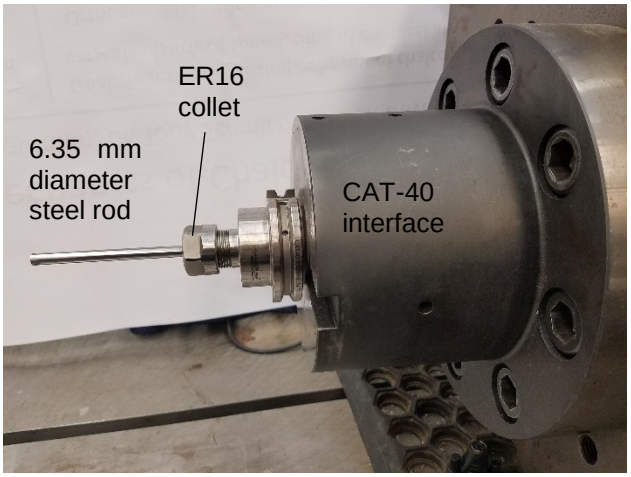

Figure 4. 6.35 mm diameter rod setup.

For both rod diameters, multiple stickout lengths were selected and measurements were performed with: a medium-size accelerometer (PCB 352A21), a small-size accelerometer (PCB 352C23), and a laser vibrometer (Polytec OFV-534). The latter provided a non-contact measurement reference with no mass loading. To obtain the accelerometer-cable masses, measurements were performed using an Ohaus AV264C Adventurer ProAnalytical Balance (0.1 mg resolution).

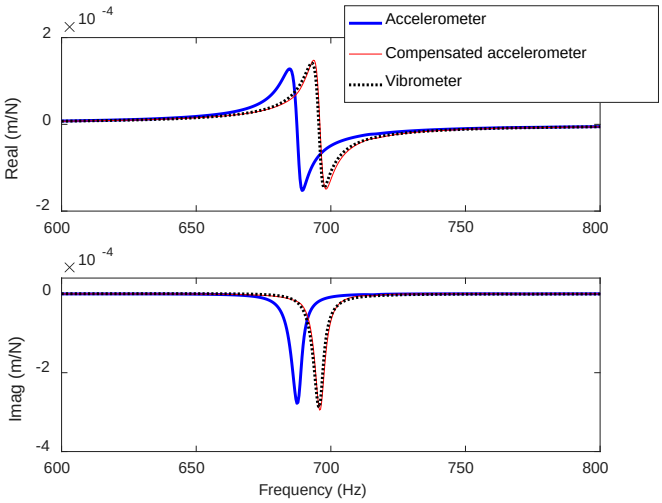

Figure 5. Results for 12.7 mm diameter rod with a stickout length of 102 mm using the medium accelerometer.

Figure 5 shows the measurement and compensation results for the 12.7 mm diameter rod with a stickout length of 102 mm using the medium accelerometer, where the accelerometer-cable mass was 706 mg. It is seen that the accelerometer FRF has a lower natural frequency than the vibrometer (non-contact)

FRF. Using Eq. 2 and the measured mass, the mass-loaded FRF was compensated to remove the mass loading effect. This result matches closely with the vibrometer result (the phase error in the vibrometer measurement due to a small time delay between the hammer and vibrometer amplifying electronics was compensated using the technique described in [19]).

A summary of the 12.7 mm diameter rod measurement results for both accelerometers at four different stickout lengths is provided in Table 1. The average percent error in the compensated result for all tests is 0.005%. Prior to compensation, the percent error in natural frequency for the medium accelerometer was 1.0% and 0.4% for the small accelerometer.

Table 1. 12.7 mm diameter rod mass compensation results.

Stick -out (mm)	Vibr. natl. freq. (Hz)	Accel. natl. freq. (Hz)	% error	Comp. natl. freq. (Hz)	% error
Medium accelerometer (706 mg)					
102	695.4	687.4	1.10	695.8	-0.05
111	597.8	592	0.97	598.5	-0.11
118	538.3	533.3	0.92	537.5	0.15
124	492.1	487.1	1.01	492.1	0
Small accelerometer (275 mg)					
102	698.1	695	0.44	698.1	0
111	613.8	611.5	0.37	614.2	-0.06
118	555.4	552.8	0.46	555	0.07
124	503	501.3	0.33	502.8	0.03

Measurement results for the 6.35 mm diameter rod are presented in Table 2. The average percent error in the compensated results for all tests is -0.09%. Prior to compensation, the percent error in natural frequency for the medium accelerometer was 5.8% and 2.4% for the small accelerometer.

Table 2. 6.35 mm diameter rod mass compensation results.

Stick -out (mm)	Vibr. natl. freq. (Hz)	Accel. natl. freq. (Hz)	% error	Comp. natl. freq. (Hz)	% error
Medium accelerometer (680 mg)					
79	688.2	646.0	6.1	688.9	-0.10
89	546.3	516.0	5.5	547.0	-0.13
Small accelerometer (275 mg)					
79	687.8	671.0	2.4	688.2	-0.06
89	545.5	532.2	2.4	545.9	-0.07

*Stickout lengths are approximate. Different setups were used between the small and medium accelerometers.

In addition to the 6.35 mm diameter rod measurements, experiments were also performed on two clamped-clamped-clamped-free boundary condition thin ribs. The 6.35 mm diameter rod and ribs represent examples of flexible structures that may have both their FRF natural frequency(s) and amplitudes affected by the contact measurement approach. For the ribs, one rib material was 6061-T6 aluminum and the other was 6Al-4V titanium. The titanium rib was approximately an order of magnitude stiffer than the aluminum rib at the center of the unsupported edge. The small accelerometer and laser vibrometer were used for the rib measurements. The setup is shown in Fig. 6, where the thin ribs were fixed to the table using cyanoacrylate and the measurement location was the center of the unsupported edge.

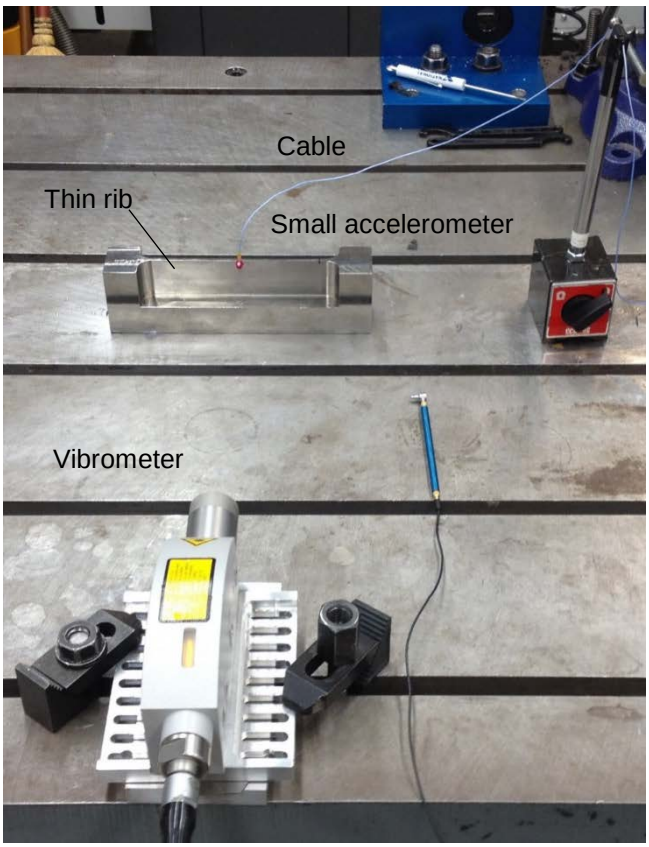

Figure 6. Thin rib setup.

Figures 7-9 display measurement and compensation results. In Fig. 7, FRFs for the 6.35 mm diameter rod with a stickout length of 89 mm are displayed. It is seen that the accelerometer-based FRF has a lower natural frequency (due to the mass loading) and a reduced amplitude (due to the cable damping). The measured accelerometer-cable mass was substituted in its modeled receptance and the damping

coefficient was adjusted to provide an amplitude match between the compensated FRF and vibrometer FRF. The aluminum and titanium rib results are shown in Figs. 8 and 9. The mass loading and damping compensation results for the 6.35 mm diameter rod and both ribs are summarized in Table 3.

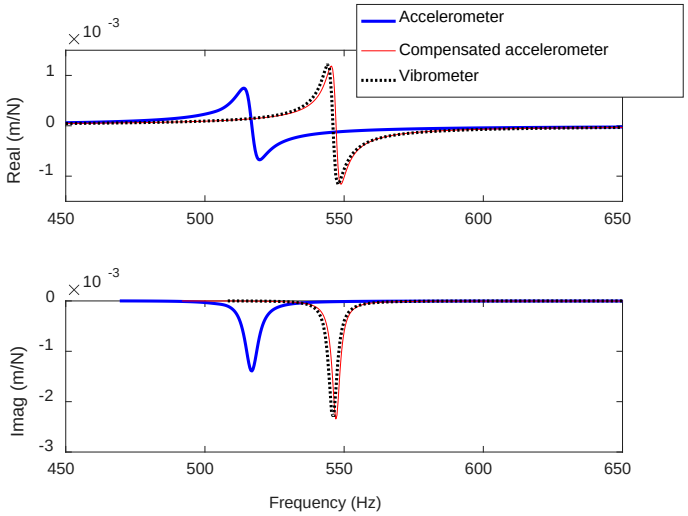

Figure 7. 6.35 mm diameter rod results for medium accelerometer with 89 mm stickout length.

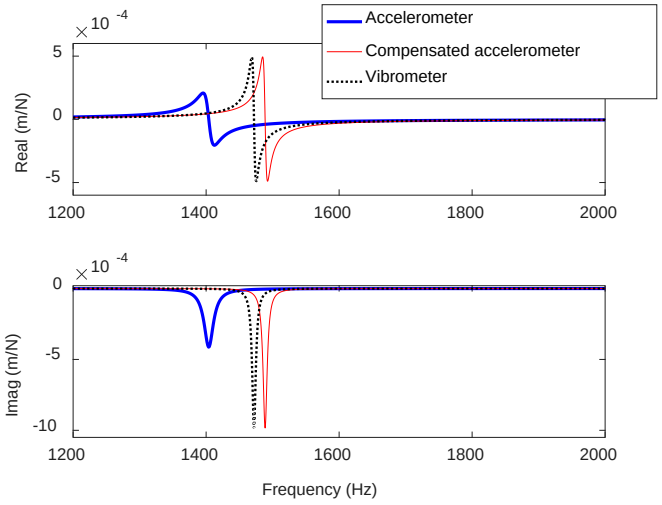

Figure 8. Aluminum rib results.

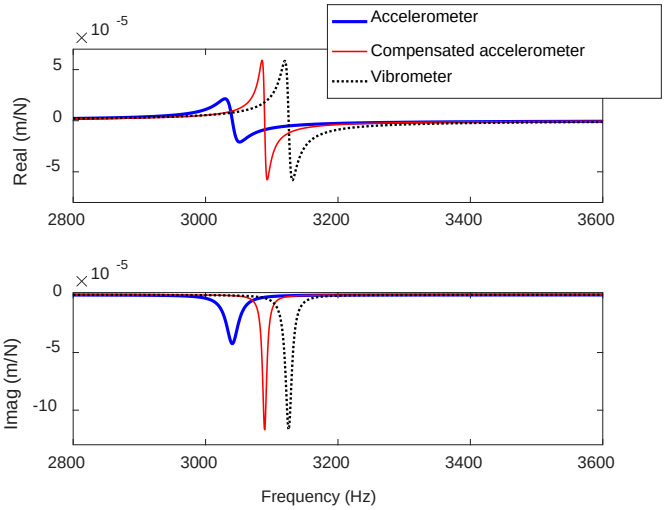

Figure 9. Titanium rib results.

Table 3. Mass loading and damping compensation results.

Struc-ture	Vibr. natl. freq. (Hz)	Accel. natl. freq. (Hz)	% error	Comp. natl. freq. (Hz)	% error	c (N-s/m)
6.35 mm rod	Medium accelerometer (680 mg)					
79 mm	688.2	646.0	6.1	688.9	-0.10	0.13
89 mm	546.3	516.9	5.4	547.0	-0.13	0.15
6.35 mm rod	Small accelerometer (275 mg)					
79 mm	687.8	671.0	2.4	688.2	-0.06	0.07
89 mm	545.5	532.2	2.4	545.9	-0.07	0.07
Rib	Small accelerometer (286.4 mg)					
Al 6061-T6	1472	1404	4.6	1488	-1.13	0.17
Ti 6Al-4V	3125	3040	2.7	3089	1.16	0.85

Although this does not represent a comprehensive study of cable damping effects, conclusions can be drawn from Table 3. First, for a single structure and a single accelerometer, the damping value was consistent. Specifically, 1) c = 0.07 N-s/m for both 6.35 mm diameter rod measurements using the small accelerometer; and 2) c = 0.13 N-s/m and 0.15 N-s/m for the 6.35 mm diameter rod measurements using

the medium accelerometer. Presumably, the change is c values is due to the difference in cables and/or cable configuration between the two accelerometers/setups.

Second, the *c* value may scale with the structure's stiffness. Of the three structures, the 6.35 mm diameter rod was the most flexible, followed by the aluminum rib, and, finally, the titanium rib. Considering the small accelerometer, the *c* values increase from 0.07 to 0.17 to 0.85, respectively, for these three setups. Future testing will focus on an improved understanding of the viscous damping coefficient required to compensate for cable-based energy dissipation.

CONCLUSIONS

This paper described the application of inverse Receptance Coupling Substructure Analysis (RCSA) to mass and damping compensation for accelerometer-based impact testing. The measurement (assembly) FRF was used together with a point mass-viscous damping model of the accelerometer-cable to determine the compensated tool point FRF using the analytical inverse RCSA approach. Experiments were completed for: 1) two rod diameters and multiple stickout lengths for clamped-free rod boundary conditions; and 2) thin ribs with clamped-clamped-clamped-free boundary conditions. The average percent error in compensated natural frequency over all 14 tests reported in this study was -0.02%.

A limitation to the compensation procedure is that a first-principles approach to predict the viscous damping coefficient based on cable properties is not presented. However, the absence of physics-based models is true, in general, for mechanical damping in structures. Consider finite element analysis, for example. The eigensolution (natural frequencies and mode shapes) can be predicted quite accurately if boundary conditions are properly described. However, if scaled FRFs are desired, the damping type and values must be entered based on the user's prior experience. The approach presented here provides a mechanism for incorporating damping, as well as mass, in FRF compensation and motivates future work to approximate, tabulate, and (potentially) model the cable behavior.

ACKNOWLEDGEMENTS

This material is based upon work supported by the National Science Foundation under Grant No. CMMI-1561221.

REFERENCES

[1] Tlusty, G., 2000, Manufacturing Processes and Equipment, Prentice Hall, Upper Saddle River, NJ.

[2] Altintas, Y., 2000, Manufacturing Automation: Metal Cutting Mechanics, Machine Tool Vibrations, and CNC Design, Cambridge University Press, Cambridge, UK.

[3] Schmitz, T.L. and Smith, K.S., 2009, Machining Dynamics: Frequency Response to Improved Productivity, Springer, New York, NY.

[4] Schmitz T.L. and Donaldson R.R., 2000. Predicting High-Speed Machining Dynamics by Substructure Analysis, CIRP Annals-Manufacturing Technology, 49/1: 303-308.

[5] Schmitz, T., Davies, M., Medicus, K., and Snyder, J., 2001, Improving High-Speed Machining Material Removal Rates by Rapid Dynamic Analysis, Annals of the CIRP, 50/1: 263-268.

[6] Schmitz, T., Davies, M., and Kennedy, M., 2001, Tool Point Frequency Response Prediction for High-Speed Machining by RCSA, Journal of Manufacturing Science and Engineering, 123: 700-707.

[7] Duncan, G.S., Tummond, M., and Schmitz, T., 2005, An Investigation of the Dynamic Absorber Effect in High-Speed Machining, International Journal of Machine Tools and Manufacture, 45: 497-507.

[8] Schmitz, T. and Duncan, G.S., 2005, Three-Component Receptance Coupling Substructure Analysis for Tool Point Dynamics Prediction, Journal of Manufacturing Science and Engineering, 127/4: 781-790.

[9] Schmitz, T. and Duncan, G.S., 2006, Receptance Coupling for Dynamics Prediction of Assemblies with Coincident Neutral Axes, Journal of Sound and Vibration, 289/4-5: 1045-1065.

[10] Schmitz, T., Powell, K., Won, D., Duncan, G.S., Sawyer, W.G., and Ziegert, J., 2007, Shrink Fit Tool Holder Connection Stiffness/Damping Modeling for Frequency Response Prediction in Milling, International Journal of Machine Tools and Manufacture, 47/9: 1368-1380.

[11] Cheng, C.-H., Duncan, G.S., and Schmitz, T., 2007, Rotating Tool Point Frequency Response Prediction using RCSA, Machining Science and Technology, 11/3: 433-446.

[12] Filiz, S., Cheng, C.-H, Powell, K., Schmitz, T., and Ozdoganlar, O., 2009, An Improved Tool-Holder Model for RCSA Tool-Point Frequency Response Prediction, Precision Engineering, 33: 26-36.

[13] Schmitz, T., 2010, Torsional and Axial Frequency Response Prediction by RCSA, Precision Engineering, 34: 345-356.

[14] Kumar, U. and Schmitz, T., 2012, Spindle Dynamics Identification for Receptance Coupling Substructure Analysis, Precision Engineering, 36/3: 435-443.

[15] Ewins, D.J., 2009, Modal Testing: Theory, Practice and Application, 2nd Ed., Wiley, New York, NY.
[16] Özşahin, O., Özgüven, H.N., and Budak, E., 2010, Analysis and Compensation of Mass Loading Effect of Accelerometers on Tool Point FRF Measurements for Chatter Stability Predictions, International Journal of Machine Tools and Manufacture, 50/6: 585-589.
[17] Olvera, D., Elías-Zúñiga, A., Martínez-Romero, O., de Lacalle, L.L., Martínez-Alfaro, H., Siller, H.R., and Pineda, M.W., 2016, Improved Predictions of the Stability Lobes for Milling Cutting Operations of Thin-wall Components by Considering Ultra-miniature Accelerometer Mass Effects, The International Journal of Advanced Manufacturing Technology, 86/5-8: 2139-2146.
[18] Schmitz, T.L. and Smith, K.S., 2012, Mechanical Vibrations: Modeling and Measurement. Springer, New York, NY.
[19] Ganguly V. and Schmitz T.L., 2014, Phase Correction for Frequency Response Function Measurements, Precision Engineering, 38: 409-413.